

Article

Assessment of the Thermal Properties of Buildings in Eastern Almería (Spain) during the Summer in a Mediterranean Climate

María Paz Sáez-Pérez ^{1,*} , Luisa María García Ruiz ²  and Francesco Tajani ³ 

¹ Building Constructions Department, Advanced Technical School for Building Engineering, University of Granada, 18071 Granada, Spain

² International School for Postgraduate Studies, University of Granada, 18071 Granada, Spain; lumagr@correo.ugr.es

³ Department of Architecture and Design, Sapienza University of Rome, 00185 Roma, Italy; francesco.tajani@uniroma1.it

* Correspondence: mpsaez@ugr.es

Abstract: Within a context in which temperatures are increasing due to global warming, it is important to assess the capacity of buildings, old and modern, to respond to this new situation. Recent studies have highlighted the importance of understanding more about the thermal properties of traditional constructions. This study quantifies the impact of the high summer temperatures typical of the Mediterranean climate on traditional farmhouses in Eastern Almería (Spain). The study group of farmhouses was divided into three models representative of the different types of Eastern Almería vernacular architecture. Energy consumption in the three models was simulated using EnergyPlus. The three models were assessed in free-floating conditions. The window-to-wall ratio and U-factor values were studied in order to evaluate potential benefits in terms of energy efficiency. Outdoor and indoor temperatures were compared. Finally, an adaptive thermal comfort analysis was performed according to ASHRAE 55. Results highlight the ability of Eastern Almería farmhouses to mitigate extreme temperatures.

Keywords: Mediterranean architecture; energy simulation; window-to-wall ratio; thermal transmission; thermal comfort



Citation: Sáez-Pérez, M.P.; Ruiz, L.M.G.; Tajani, F. Assessment of the Thermal Properties of Buildings in Eastern Almería (Spain) during the Summer in a Mediterranean Climate. *Sustainability* **2024**, *16*, 746. <https://doi.org/10.3390/su16020746>

Academic Editors: Xiaolei Yuan, Risto Kosonen, Yizhe Xu, Weixin Zhao and Gerardo Maria Mauro

Received: 6 September 2023

Revised: 11 December 2023

Accepted: 10 January 2024

Published: 15 January 2024



Copyright: © 2024 by the authors. Licensee MDPI, Basel, Switzerland. This article is an open access article distributed under the terms and conditions of the Creative Commons Attribution (CC BY) license (<https://creativecommons.org/licenses/by/4.0/>).

1. Introduction

Climate change is producing high global warming in a short period of time, causing health, the economy and the environment to be negatively affected, such as the heat waves present in large cities [1–3]. This situation especially affects the Mediterranean area, whose temperatures exceed the global average by 1.4 °C [4]. Therefore, it is necessary for buildings to mitigate these effects and respond to future needs [4,5]. Currently, the main factor responsible for climate change is energy, which represents 60% of greenhouse gas (GHG) emissions. Therefore, the UN establishes in its 2030 Agenda the need to guarantee access to affordable, safe, sustainable and modern energy. This is related to the improvement of energy efficiency [6].

Numerous investigations today focus on knowing the energy conditions of buildings to detect energy efficiency [7–12]. Estimating energy efficiency has been the subject of research since the late 1980s, as there was already awareness that the energy performance of the building is decisive for this [13,14]. In the 1990s, the thermal response to heat input was identified; as a consequence, in the 2000s, work began with energy models to estimate thermal parameters through simulations [15–17]. In the 2010s, computer programs were developed to perform these energy simulations to quantify the energy savings of buildings and verify the results obtained in simplified models [18–20]. In recent years, it has been confirmed that the energy performance of buildings is conditioned by their

physical characterization, which is why the aim is to estimate different climatic situations, a fact that especially benefits residential typology [13,21].

The parameters that allow thermal characterization and its simulation are the Window-to-Wall Ratio (WWR), which is the percentage of transparent area in the façades with respect to their opaque area, and the U-factor, which is the amount of heat transferred from the exterior to the interior of buildings through their construction elements. The parameter that quantifies thermal comfort conditions is the operating temperature according to ASHRAE 55 (2020) [22]. There are numerous investigations that study the thermal impact of the WWR through simulations [23–26]. The U-factor is used in many studies to quantify the capacity of buildings to conserve energy inside through simulations [27–30]. Regarding thermal comfort conditions, energy demand is defined as the energy necessary to maintain the comfort requirements inside the building (CTE HE 1, 2022) [31]. For this reason, the building envelope is studied as a key piece of its thermal behavior through simulations on White-Box Models [32–37]. Residential buildings are one of the main emitters of GHG, therefore, the main objective is not only to achieve zero emissions, but also to achieve energy improvement [38–43]. Along these lines, solutions for economic and environmental improvement are analyzed [38–48].

The aforementioned studies confirm the importance of energy evaluation of buildings through simulation, especially studies of unique buildings conditioned by their location or level of protection. No recent research has been found on the Mediterranean farmhouse. Therefore, there is a need to know its energy efficiency to guide the decision-making process towards climate change and adapt heritage to global warming. The specific contribution of the work is evaluating the thermal capacity of the Mediterranean farmhouse and quantifying the benefits of its physical configuration through White-Box Models representative of the farmhouses located in the rural environment of eastern Almería. The novelty of the work with respect to the existing literature is specified in the results by providing premises to develop strategies that adapt to current uses with good performance in the face of extreme climatic events. The article is structured in four phases: first, the characterization of the representative type models of the Mediterranean farmhouse is addressed; second, the methodology for evaluating the models is detailed; third, the results are presented and discussed regarding the benefits of the Mediterranean farmhouse to mitigate climate change; and fourth, the conclusions are addressed.

2. Literature Review

Various research focuses on understanding the consumption and energy efficiency performance of historic buildings through simulations [48–54]. However, it is important to focus on vernacular architecture studies, especially traditional homes, whose comfort conditions do not respond to a universal model, but rather undergo constant evolution depending on the climate and their location [55,56]. In this typology, initially and due to the absence of means, the optimization of behavior was achieved through passive strategies; however, the modernization of the construction sector is causing the loss of knowledge of bioclimatic design [57], and along with this comes the misuse of what exists.

Keeping the existing stock of traditional buildings and vernacular Mediterranean architecture involves several benefits. In Mediterranean countries, the farmhouse is the representative typology of vernacular housing, considered a rural construction linked to agricultural exploitation and built with local materials. They present a geometry compatible with new and current uses, a fact in which lies their potential for reuse [58–60]. There are energy studies in which the typology of farmhouses in Mediterranean countries is studied [4,61–65]. Furthermore, the bioclimatic design of vernacular architecture has been evaluated and quantified through energy simulations [66–71]. The modeling procedure in the OpenStudio application for SketchUp and the simulation using the EnergyPlus 8.6.0 software are common in the evaluation of energy consumption in buildings [39,72–79] and in research related to natural ventilation [80,81]. The potential of the tool for climatic, thermal and hygrothermal studies is also the subject of study [82–87]. Another line of

research related to vernacular housing in Mediterranean countries pursues the optimization of its thermal performance through the implementation of new materials [88,89] and the quantification of the heat transmission of its envelope [90].

3. Case Study

Vernacular architecture typically involves the use of local building materials and techniques that adapt to the particular circumstances of the local climate. It is therefore extremely heterogeneous [91,92]. The traditional Mediterranean dwelling located in rural and coastal regions [93] has been studied in numerous countries in the Mediterranean Basin, such as Cyprus [63,93,94], Greece [95], Italy [96,97], Spain [98,99] and Israel [100]. Similar constructions have also been studied in countries outside the Mediterranean region, such as Ghana [91].

The typical characteristics of traditional Mediterranean housing include thick walls and white lime-washed façades [96]. Sometimes, they also have inner courtyards as open-air private spaces [100]. Regarding doors and windows, these vary according to the particular region, as can be deduced from [100], who affirmed that façades typically contained just a few small window openings, in contrast to [101], who calculated a high WWR in the façades. Within the existing variants, in this research we will be studying the typical Mediterranean farmhouse in the eastern part of the province of Almería in SE Spain. From our on-site inspections, we found that these houses are normally located on a wide expanse of land suitable for cultivation that lies close to a water channel. The houses have either one or two floors. In the latter case, the upper floor does not normally occupy the entire area of the ground floor. The rooms intended for residential use are generally south- and east-facing, while those originally intended for keeping livestock and farm tools, are mostly oriented towards the north and west. The south façades have more and larger window openings while there are fewer, smaller ones on the north façades. In terms of building materials, the walls are made with limestone masonry and lime mortar and finished with a lime render. They are normally between 40 and 70 cm thick. There is no single criterion for the roof. Some have flat roofs covered with a lime mortar, while others have sloping roofs covered with ceramic tiles.

Figure 1 shows traditional Mediterranean houses from Eastern Almería locations.



Figure 1. (a) Doña Jacoba farmhouse, Huércal Overa (Almería). (b) Management House of the Marqués de Chávarri, Mojácar (Almería). (c) House of Los Fuentes, Carboneras, (Almería). (d) Cortijo Morata, Vera (Almería). (e) La Providencia Winery, Antas (Almería). (f) Farmhouse Cayuela, Níjar (Almería).

3.1. Characterization of the Study Cases

The sample group studied in this research is made up of 27 farmhouses located in coastal municipalities in the province of Almería. In Table 1, the farmhouses have been classified into groups according to the number of floors, the surface area and the thickness of the exterior walls.

Table 1. Factors used to classify the sample group: number of floors; surface area; thickness of the exterior walls.

Specimens		
Floors	1 floor	15
	2 floors	9
	3 floors	3
Surface	Surface < 500 m ²	11
	500 m ² < Surface < 1000 m ²	9
	Surface > 1000 m ²	7
Thickness	45 cm	3
	50 cm	20
	65 cm	4

Table 2 shows that more than half of the sample farmhouses have a single floor and the rest have two or three floors. Regarding the surface, most of the sample farmhouses have a surface area of less than 500 m² and the majority of farmhouses analyzed have a wall 50 cm thick. The sample is divided into three groups according to the characteristics of Table 1, and representative models are made. Since the differences between specimens with different surfaces are minimal, a model is designed in each range (see Figure 2). Two single-floor farmhouses, one with a flat roof and one with a sloping roof, and a two-floor farmhouse with a flat roof are modeled. The wall thickness also varies in the three models with the intention of quantifying its influence on the results.

Table 2. Classification of the sample group. Distinguishing characteristics of each type and number of houses.

	Model Type 1	Model Type 2	Model Type 3
Identifying characteristics	1 floor Surface < 500 m ² 45 cm thick walls Flat roof	2 floors 500<Surface<1000 m ² 50 cm thick walls Sloping roof	2 floors Surface > 1000 m ² 65 thick walls Flat roofs
Specimens	11 specimens 41% of the sample	9 specimens 33% of the sample	7 specimens 26% of the sample

The WWR of the façades of the buildings (see Table 3) is determined by the total area of the window openings (Sh) and the total area of the façade (Sf) expressed in Equation (1):

$$WWR = Sh/Sf \times 100 [\%] \quad (1)$$

In Model Type 1, the WWR is less than 10% in all four façades, with a minimum value of 4.29% in the south façade and a maximum value of 8.43% in the west façade. The lowest value is on the south façade of Model Type 1, at 4.29%, and the highest value is on the east façade of Model Type 2, a 35.47%. It is worth highlighting the particularity of Model Type 3: its northern façade is the one with the highest WWR; this is because its geometry is made up of an addition of volumes. The main volume is larger than that of the adjoining rooms,

which correspond to a later construction and which, according to the sample analyzed, were smaller in size and, consequently, had a smaller WWR.

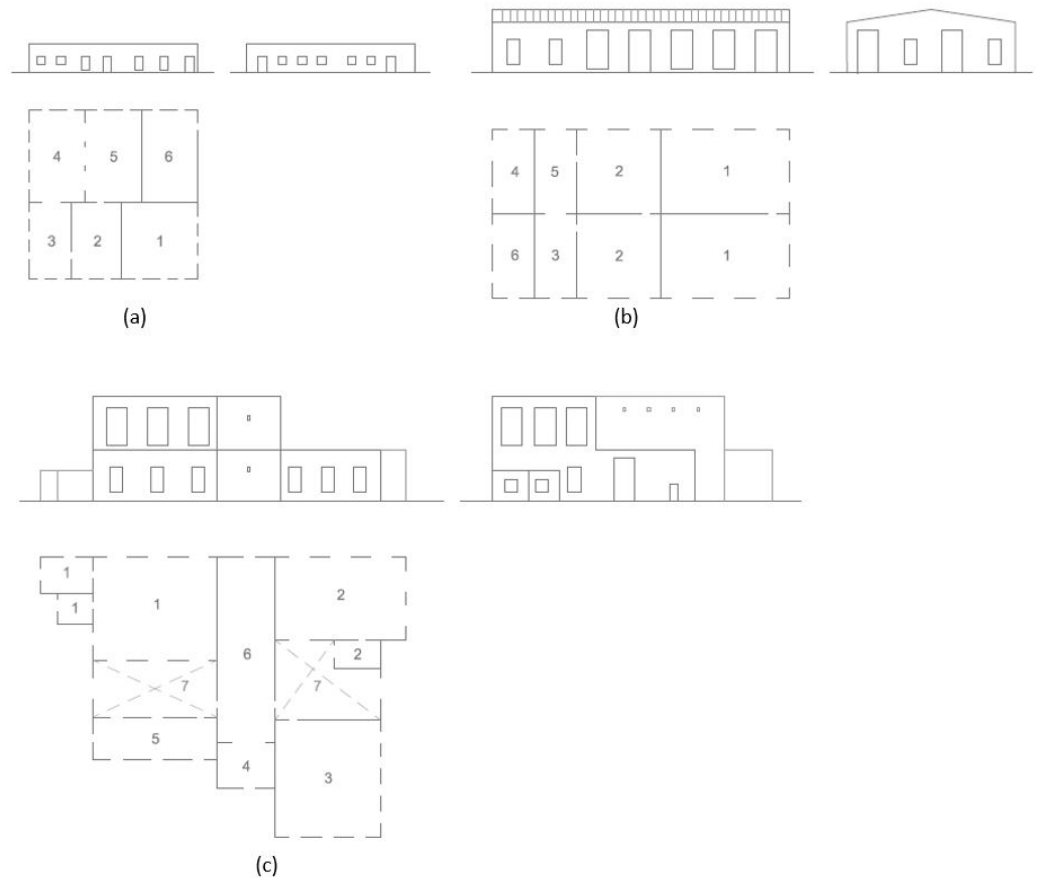


Figure 2. Layout of the three models. (a) Model Type 1 with flat roof. (b) Model Type 2 with sloping roof. (c) Model Type 3 with flat roof. Spaces: (1) Main house. (2) Laborer’s room. (3) Warehouse. (4) Pen. (5) Stable. (6) Hayloft. (7) Yard.

Table 3. WWR for the four façades in the three models classified according to CTE DB HE (2022) [31].

Model	South	East	North	West
Type 1	4.29%	7.14%	7.14%	8.43%
Type 2	21.68%	35.47%	30.65%	7.36%
Type 3	16.53%	12.02%	22.12%	11.15%

WWR ranges established in CTE DB HE (2022) for limit transmittance values
WWR: ■ 0–10% ■ 11–20% ■ 21–30% ■ 31–40%

The importance and usefulness of calculating the WWR of the façades is demonstrated in the decisive role that WWR plays in the U-factor of the façades. The U-factor is calculated according to Equation (2).

$$U = 1/Rt \tag{2}$$

where R_t ($\text{m}^2 \cdot \text{K} / \text{W}$) is the sum of different (convection and conduction) thermal resistances for all the layers of the particular construction element (roof, wall, etc.) and for the layers of indoor and outdoor air, as shown in Equation (3).

$$R_t = R_{si} + \sum R_{ti} + R_{se} \quad (3)$$

where R_{si} and R_{se} are the surface thermal resistances corresponding to the indoor and outdoor air, respectively, for vertical enclosures and horizontal heat flow, with values of $R_{si} = 0.13 \text{ m}^2 \text{ K/W}$ and $R_{se} = 0.04 \text{ m}^2 \text{ K/W}$ according to CTE [31]. The thermal resistance of each layer is calculated as follows in Equation (4).

$$R_t = e/\lambda \quad (4)$$

where e (m) is the thickness of the layer and λ ($\text{W}/(\text{m} \cdot \text{K})$) is the thermal conductivity of the material.

The regulations applicable in the geographical area in which the buildings are located, CTE DB HE (2022) [31], establish limits for the U factor values for each construction element so as to guarantee thermal comfort inside the buildings. Although in this research we are studying historical buildings, we decided to use the values set out in current regulations because the aim was to assess whether these buildings are compatible with current uses.

3.2. Location of Case Studies and Climate Analysis

The farmhouses in our case study are located in the province of Almería on the Mediterranean coast in southeast Spain, a semi-arid area with an average annual rainfall in its different regions of between 380 and 760 mm. This results in a hot, dry climate with an average annual temperature of over $18 \text{ }^\circ\text{C}$ [102,103]. The farmhouses are situated at an average altitude of 356 m above sea level.

This climate in the Mediterranean as a whole can be categorized as a warm temperate or mesothermal climate, with an average temperature of $8 \text{ }^\circ\text{C}$ in the coldest month and $25 \text{ }^\circ\text{C}$ in the warmest month. The western Mediterranean is characterized by dry summers with an average maximum temperature of $25 \text{ }^\circ\text{C}$.

The CTE DB HE (2022) [31] standard classifies the different parts of Spain into climatic zones based on the province and its altitude above sea level, for the purpose of defining the exterior parameters in a typical year that may be used in the calculations in relation to possible energy savings. In this case study, as the province is Almería and the farmhouses are located within the altitude range of 351 to 400 m above sea level, the study area is classified as climate zone B3. The letter B indicates a mild winter climate with a severity of between 0.23 and 0.5, while the number 3 indicates a harsh summer climate with a severity value of between 0.83 and 1.38. This study focuses on the summer months, the period with the highest temperatures in this area, in order to assess the thermal behavior of these buildings when exposed to the most unfavorable conditions. In the course of this research, we used temperature data for the year 2022, the most recent year for which all the information is available.

4. Methodology

4.1. The Simulation: The Numerical Study

The three models were subjected to an energy simulation, in order to assess their thermal behavior in a “free floating” state, that is, without the support of artificial air conditioning, ventilation, heating or cooling systems. In this simulation, the EnergyPlus 8.6.0 software, a tool that offers reliable results, was used through the OpenStudio application for SketchUp. The first stage was to enter the geometric data for the models defined by the SketchUp 2019 software, namely the envelopes, openings and perimeters of their construction elements, differentiating between interior, exterior and areas in contact with the ground. The modeling also takes into account the orientation of each farmhouse for obtaining reliable self-shadows. In this stage, thermal bridges located at the junctions of

the enclosure with the openings are considered, and they are modeled using subsurfaces in the enclosure. These subsurfaces are assigned the value of an equivalent surface thermal transmittance (U_p) to the linear thermal transmittance characteristic of each thermal bridge. This equivalence is obtained from Equation (5):

$$U_p = \Psi/h, \quad (5)$$

where:

U_p is the equivalent surface thermal transmittance (W/m^2K) of the thermal bridge.

Ψ is the linear thermal transmittance (W/mK) of the thermal bridge. Tabulated values in CTE DB HE3 [31].

h is the length equivalent to the dimension of the existing thermal bridge (m).

Secondly, the thermal characteristics of each model were defined using the OpenStudio 1.1.0 application, specifying the boundaries of the various thermal zones. Given that the models do not have an air conditioning system, a free-floating simulation was performed. It is assumed that the three models are unoccupied, as is the case in studies such as [99], in order to obtain results unaffected by potential ventilation or curtain manipulation, which could be caused by occupants. In this scenario, it accurately reflects reality, as a significant portion of the studied sample consists of uninhabited constructions. Table 4 shows the thermal properties considered for the envelope building materials taken from [103], except for single glass windows, whose thermal properties are available in the software database.

Table 4. Thermal properties considered for the materials in the building envelopes.

	Conductivity (W/mK)	Specific Heat (J/kgK)	Solar Absorptance
Masonry	1.06	1000	0.30
Lime	1.00	1000	0.92
Plaster	0.80	1000	0.40
Wood	0.15	1600	0.50
Topsoil	0.52	1840	0.50
Ceramic tile	1.00	800	0.50

Finally, the EnergyPlus 8.6.0 energy simulation tool was applied using the previously entered data together with the outdoor temperature data for the province of Almería (Spain) provided by the developers of this tool. At the same time, the values for the different parameters were obtained. These included U-factor and WWR values, together with the maximum, average and minimum daily temperatures during the summer period and the adaptive thermal comfort analysis, as defined by the standard ASHRAE 55 (2020) [22]. Figure 3 shows the procedure followed.

1. Enter the geometric data:
 - Define construction elements.
 - Differentiate interior, exterior and areas in contact with the ground.
2. Define the thermal characteristics of the models:
 - Specify boundaries of the thermal zones.
 - Do not specify an air conditioning system for a free-floating model.
3. Perform the energy simulation:
 - Use the previously entered data.
 - Use the outdoor temperature data for the province of Almería (Spain).
4. Obtain the values for the different parameters:
 - U-factor.
 - WWR values.
 - Maximum, minimum and average daily temperatures.
 - Adaptive Thermal Comfort Analysis.

Figure 3. Outline of the procedure.

It is important to note that Models Type 1 and 2 (MT1 and MT2) have a single thermal zone for which a single set of thermal behavior results are obtained. However, Model Type 3 is made up of a sum of volumes and must therefore be approached in two different ways: firstly, by calculating average values (simplified MT3 = equivalent to a single thermal zone) to enable its comparison with the other two models (MT1 and MT2); and secondly, as an independent model establishing a comparison between its different spaces (detailed MT3).

Figure 4 shows the monitored external temperature and the external temperature from the climatic data available in AEMET [104], taken from the Huércal-Overa Meteorological Station (Almería), as it is the closest to the sample location, at 7.4 km away. Additionally, it is the only municipality where there are specimens of the sample with a meteorological station. It is situated at an altitude of 300 m, representing a difference of 56 m compared to the average altitude of the sample. In this research, official AEMET [104] data is utilized, as there is an observation that there are no significant differences of more than 3 °C between the two datasets. In Figure 4, a range of temperatures and temperature differences between consecutive days is observed, characteristic of the sub-arid features of the Mediterranean climate variant in the province of Almería.

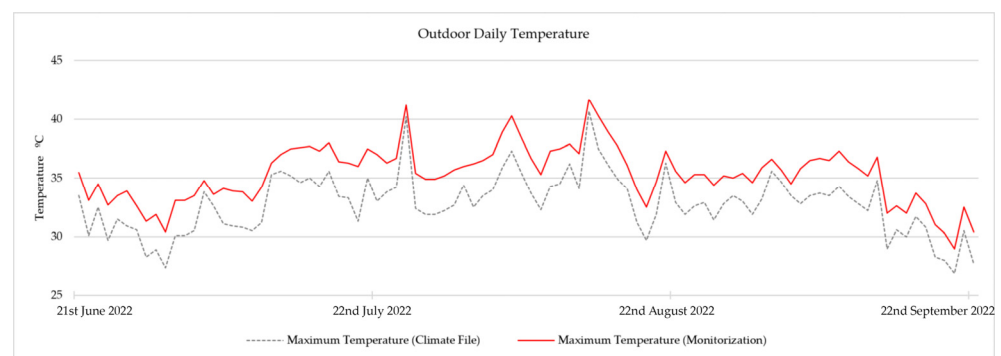


Figure 4. Thermal difference between the climatic data available from AEMET [104] and the monitored temperature.

4.2. Calibration and Validation of the Model Types

The three models were monitored from 21 June 2022 to 22 September 2022, using the Elitech RC-5+ temperature monitor. For the calibration and validation of each model, the indoor air of four rooms in each model was recorded, one facing each cardinal point, to obtain an average value. The calibration and validation procedure described in [98] was followed because it serves the same purpose of studying the temperature inside the constructions. To achieve this, uncertainty indices specified in the guidelines of ASHRAE Guideline 14-2014 [105] are used, namely the Mean Bias Error (NMBE), the Coefficient of Variation of the Root Mean Square Error (CVRMSE), and the Coefficient of Determination (R^2), defined in Equations (6)–(8), respectively. For validation, monitored data are employed every hour throughout the entire study period.

$$NMBE = \frac{1}{m} * \frac{\sum_{i=1}^n (m_i - s_i)}{n} * 100 \quad (6)$$

$$CVRMSE = \frac{1}{m} * \sqrt{\frac{\sum_{i=1}^n (m_i - s_i)^2}{n}} * 100 \quad (7)$$

$$R^2 = 1 - * \frac{\sum_{i=1}^n (m_i - s_i)^2}{\sum_{i=1}^n (m_i -)^2} \quad (8)$$

where:

m = monitored temperature

s = simulated temperature

n = number of temperature data to work with.

Table 5 displays the average values for each Model Type, which adhere to the limits set by ASHRAE 14 [105].

Table 5. Statistical indices for model validation with ASHRAE.

	NMBE (%)		CVRMSE (%)		R ²	
	Model Value	ASHRAE Limit	Model Value	ASHRAE Limit	Model Value	ASHRAE Limit
Model Type 1	−7.40	±10.00	15.30	<30	0.79	>0.75
Model Type 2	−6.10	±10.00	10.20	<30	0.88	>0.75
Model Type 3	−4.20	±10.00	8.40	<30	0.93	>0.75

4.3. Adaptive Thermal Comfort According to ASHRAE 55

In this study, thermal comfort was analyzed by obtaining the adaptive thermal comfort values according to the standard ASHRAE 55 (2020) [22]. Two ranges of comfort temperatures are established based on the average outdoor temperatures. One of the ranges indicates an acceptability percentage of 80%, while the other range indicates an acceptability percentage of 90%. Equation (9) is used to obtain the ideal comfort temperature values:

$$T_0 = (T_{MT} + T_{med})/2 \quad (9)$$

where T_{MT} is the temperature of the analyzed model and T_{med} is the mean temperature inside the farmhouse. In order to analyze the most unfavorable conditions during the study period, the T_{MT} value was taken as the maximum daily value within the model. Once we had calculated T_0 , we then calculated 80 and 90% of its excess and default values to determine the acceptability percentages. Figure 5 shows the acceptability percentage ranges for the average outdoor temperature in Almería during the period considered in this study:

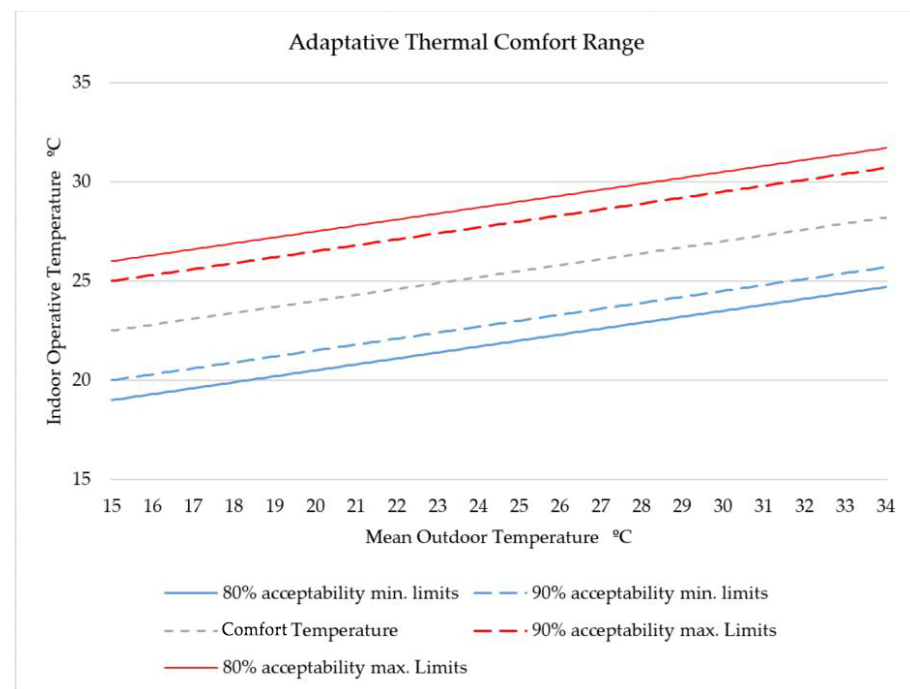


Figure 5. Acceptability percentage ranges for adaptive thermal comfort in Almería during the summer period.

5. Results

The following subsections show the results obtained from the study of the layout and the orientation of the three models.

5.1. Impact of Orientation on the Performance of the Three Models

This section presents the U-factor results for the envelope of the three models, obtained through numerical calculations as outlined in the Technical Building Code (CTE) [31]. Threshold values are included for verification purposes.

Table 6 shows the U-factor values for the construction elements in Models Type 1, 2 and 3 and the threshold values established in the CTE DB HE (2022) [31] for the climatic zone in which the study area is located.

Table 6. U-factor values for the construction elements in models and threshold values in the CTE DB HE (2022) [31].













Element	Model Type 1 (W/m ² K)	Model Type 2 (W/m ² K)	Model Type 3 (W/m ² K)	DB HE Limit (W/m ² K) (CTE, 2022)
Walls in contact with the outside air	1.54	1.43	1.19	0.56
Covers in contact with the outside	1.94	2.00	1.94	0.44
Floors in contact with the ground	5.20	5.20	5.20	0.75

It is observed that the U-factor in the walls in contact with the outside air is higher in Model Type 1, at 1.54 W/m² K, and lower in Model Type 3, at 1.19 W/m² K; these differences are due because the models have different thicknesses, being greater in Model Type 3 and lower in Model Type 1. It is observed that the U-factor in the covers in contact with the outside air is greater in Model Type 2, at 2.00 W/m² K, and, in Models Type 1 and 3, it is 1.94 W/m² K, since Model Type 2 has a sloping roof and the other two have a flat roof. In the case of soils in contact with the ground, the three standard models have the same value because the physical characteristics are identical. Comparing these values with the limits of the regulations, in all cases it is exceeded. Table 7 shows the U-factor values for the openings (doors and windows) in Models Type 1, 2 and 3 and the limit values established in the CTE DB HE (2022) [31] for the climatic zone within which the study area is classified.

In all three models, the openings obtained a U-factor value of 5.9 W/m² K. This is due to the fact that the geometric and thermal characteristics are the same in all three cases. Comparing the different limits established by the regulations based on the orientation, openings and WWR, it is observed that the values are exceeded in all the façades of the three models.













As seen previously, the CTE DB HE (2022) [31] establishes limit values for the U-factor of solid construction elements and openings based on their Window-to-Wall Ratio (WWR). However, it does not provide absolute limit values for the façade, resulting from combining the U-factor of the enclosure with the U-factor of the opening in their proportion. Nevertheless, this parameter is very useful for comparing the three models with each other. Table 8 shows the U-factor for the four façades in each model obtained from the U-factor of the solid building elements of the models (Table 6), the U-factor of the voids of the models (Table 7) and the WWR.

Table 7. U-factor values for the openings (doors and windows) in the models and threshold values in the CTE DB HE (2022) [31].

Model	South	East	North	West
Type 1 $U = 5.9 \text{ W/m}^2\text{K}$	 $U_{lim} = 5.7 \text{ W/m}^2\text{K}$	 $U_{lim} = 5.7 \text{ W/m}^2\text{K}$	 $U_{lim} = 5.4 \text{ W/m}^2\text{K}$	 $U_{lim} = 5.7 \text{ W/m}^2\text{K}$
Type 2 $U = 5.9 \text{ W/m}^2\text{K}$	 $U_{lim} = 5.7 \text{ W/m}^2\text{K}$	 $U_{lim} = 4.0 \text{ W/m}^2\text{K}$	 $U_{lim} = 3.0 \text{ W/m}^2\text{K}$	 $U_{lim} = 5.7 \text{ W/m}^2\text{K}$
Type 3 $U = 5.9 \text{ W/m}^2\text{K}$	 $U_{lim} = 5.7 \text{ W/m}^2\text{K}$	 $U_{lim} = 4.9 \text{ W/m}^2\text{K}$	 $U_{lim} = 3.3 \text{ W/m}^2\text{K}$	 $U_{lim} = 4.9 \text{ W/m}^2\text{K}$

WWR ranges established in CTE DB HE (2022) for limit transmittance values
WWR: ■ 0–10% ■ 11–20% ■ 21–30% ■ 31–40%

Table 8. U-factor for the four façades in each model.

Model	South	East	North	West
Type 1	 $U = 1.71 \text{ W/m}^2\text{K}$	 $U = 1.85 \text{ W/m}^2\text{K}$	 $U = 1.85 \text{ W/m}^2\text{K}$	 $U = 1.90 \text{ W/m}^2\text{K}$
Type 2	 $U = 2.39 \text{ W/m}^2\text{K}$	 $U = 3.00 \text{ W/m}^2\text{K}$	 $U = 2.79 \text{ W/m}^2\text{K}$	 $U = 1.75 \text{ W/m}^2\text{K}$
Type 3	 $U = 1.96 \text{ W/m}^2\text{K}$	 $U = 2.04 \text{ W/m}^2\text{K}$	 $U = 2.22 \text{ W/m}^2\text{K}$	 $U = 1.47 \text{ W/m}^2\text{K}$

WWR ranges established in CTE DB HE (2022) for limit transmittance values
WWR: ■ 0–10% ■ 11–20% ■ 21–30% ■ 31–40%

These data allow us to compare the U-factor between façades.

As expected, the U-factor value of the façade is higher than the U-factor of the solid element because it transmits more heat by having a transparent percentage and, consequently, thermal bridges. On the other hand, it is lower than that of the openings because these elements are entirely transparent. It is determined that the lowest U-factor is found on the south façade of Model Type 1, with a value of $1.71 \text{ W/m}^2 \text{ K}$, and which has the lowest WWR. The highest U-factor is found on the east façade of Model Type 2, with a value of $3 \text{ W/m}^2 \text{ K}$, which coincides with the highest WWR. As expected, the U-factors of the façades are greater than the U-factors of the solid elements and less than the U-factor of the hollow elements.

5.2. Analysis of the Interior Temperature of the Models

On the basis of the outdoor summer temperatures, the simulation produced the following thermal data for the interior temperatures for the three models. Figure 6 shows the maximum daily interior temperatures for Model Type 1, Type 2 and Simplified Type 3 and the maximum daily exterior temperatures.

Figure 6 shows the temperature difference between the outdoor and indoor of each model. Model Type 1 has a maximum daily indoor temperature of $25.8 \text{ }^\circ\text{C}$ and a maximum average daily indoor temperature during the summer period of $23.6 \text{ }^\circ\text{C}$ (± 1.97). Model Type 2 has a maximum daily indoor temperature of $29 \text{ }^\circ\text{C}$ and an average maximum daily indoor temperature during the summer period of $23.0 \text{ }^\circ\text{C}$ (± 1.89). Model Type 3 has a maximum daily indoor temperature of $30.0 \text{ }^\circ\text{C}$, with an average maximum daily indoor temperature during the summer period of $24.8 \text{ }^\circ\text{C}$ (± 2.20). If we consider that

the maximum daily outdoor temperature is 40.7 °C with an average maximum daily temperature of 32.7 °C (± 2.52), the maximum temperature for Model Type 1 is 15.2 °C lower than the outdoor temperature, the maximum temperature for Model Type 2 is 14.2 °C lower than the outside temperature and the maximum temperature for Model Type 3 is 11.2 °C lower than the outside temperature. As we can see, Model Type 1 and Model Type 2 obtain more similar values compared with Model Type 3, and are more extreme, as can be observed in the maximum and minimum peaks of the graph shown in Figure 6. Furthermore, it can be observed that Model Type 2, the only one with a sloped roof, exhibits the lowest temperature during a significant portion of this period, at 20.1 °C.

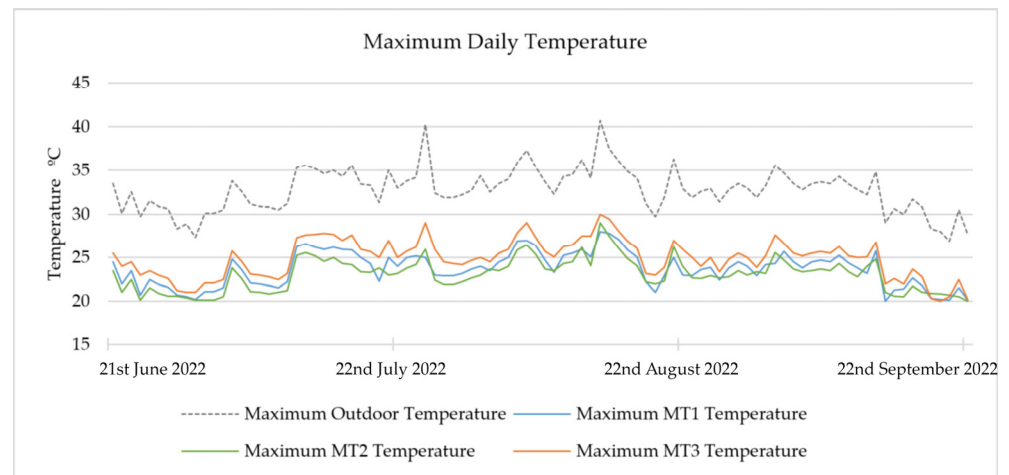


Figure 6. Maximum daily interior temperatures for Model Type 1, Type 2 and Simplified Type 3 and maximum daily exterior temperatures during the summer period.

Figure 7 shows the data for Detailed Model Type 3, i.e., the maximum values for the spaces that make up the building. Differences between the different spaces can be observed and are significant in the case of maximum temperatures. The highest, most unfavorable values were obtained for Detailed Model Type 3. Specifically, the spaces with the most unfavorable values are the upper floor of the main house, the upper floor of the hayloft and the laborer's room. For their part, the rooms with the most favorable values are the northwest annex of the main house, the ground floor of the hayloft and the ground floor of the main house. It is noted that the ceiling of the ground floor and the entire upper floor have a thermal capacity that provides thermal insulation to the ground floor.

Regarding the spaces with the most unfavorable values, we can see that the upper floor of the main house, with façades facing north, east and south, has a maximum temperature of 32 °C, and an average maximum daily temperature of 26.8 °C (± 2.16) during the summer period. The upper floor of the haystack, which has façades on all four sides, has a maximum temperature of 31.4 °C, and an average maximum daily temperature during the summer period of 26.4 °C (± 2.30). The Sharecroppers' house, with façades facing north and east, has a maximum temperature of 30.5 °C, and an average maximum daily temperature during the summer period of 25.8 °C (± 2.18). Regarding the rooms with more favorable values, the northeast annex of the main house has a maximum temperature of 28.5 °C, with an average maximum daily temperature during the summer period of 23.8 °C (± 2.26). The ground floor of the main house, facing north, has a maximum temperature of 27.6 °C, and an average maximum daily temperature during the summer period of 21.6 °C (± 2.24). Lastly, the ground floor of the haystack, with façades facing north and southwest, has a maximum temperature of 27.4 °C, and an average maximum daily temperature during the summer period of 21.5 °C (± 2.23).

Detailed Model Type 3 offers a wider range of temperatures than Simplified Model Type 3, with differences of up to 16.4 °C. This results in more days with extreme maximum temperatures.

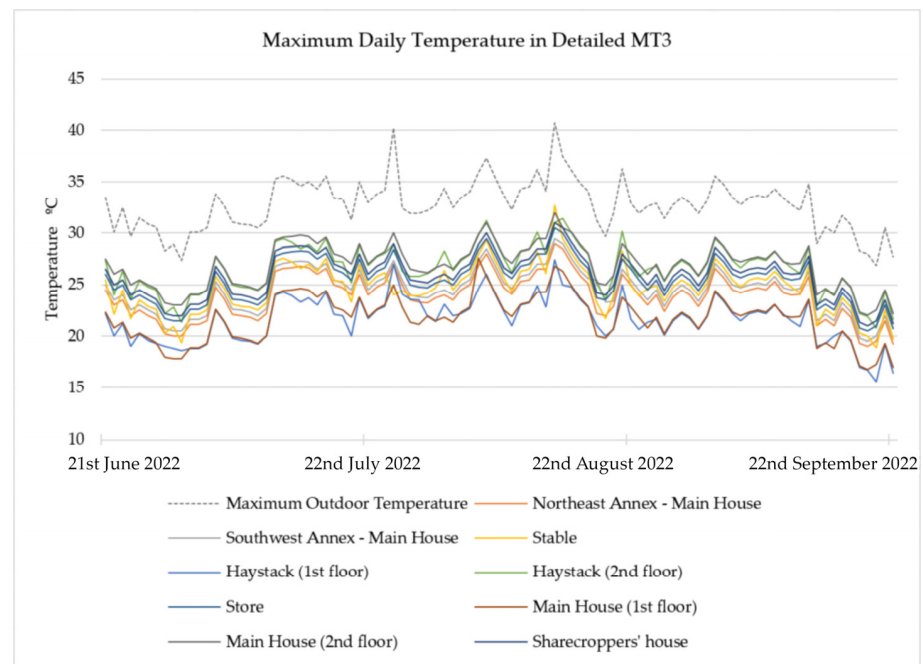


Figure 7. Maximum daily interior temperatures for Detailed Model Type 3 and maximum daily exterior temperatures during the summer period.

5.3. Adaptive Thermal Comfort in Standard Models According to ASHRAE 55

The assessment of the impact of the outdoor temperature on the thermal performance of the three models from the point of view of comfort is shown in Figures 8 and 9. They show the oscillation of the operative indoor temperature inside in relation to the average outside temperature, according to ASHRAE 55 (2020) [22].

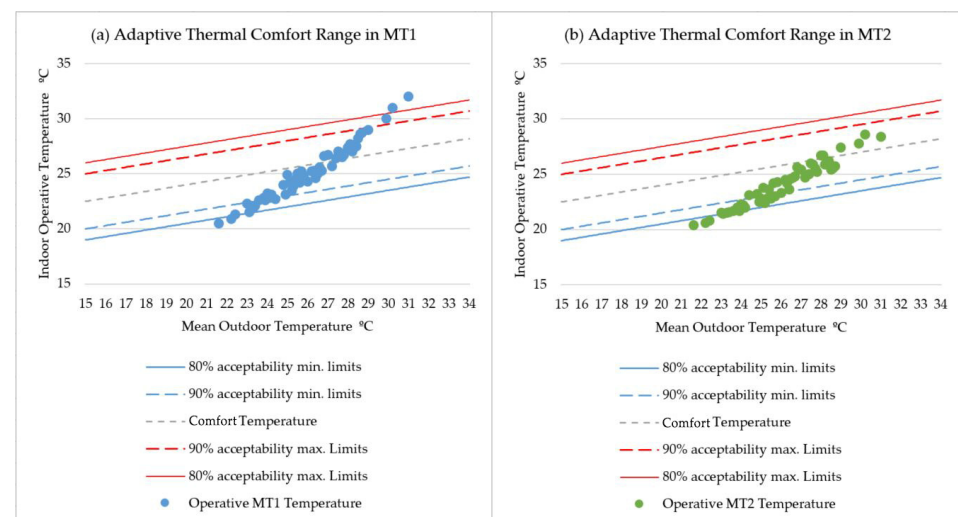


Figure 8. Adaptive thermal comfort of Models Type 1 and 2 according to ASHRAE 55 [22]. (a) Model Type 1. (b) Model Type 2.

Figure 8 shows the adaptive thermal comfort ranges established from the average outdoor temperature and the indoor operating temperatures during the summer period for Models Type 1 and 2. In Model Type 1 (Figure 8a), 15% of the days in the summer period fall outside the comfort range, 10% are within 80% acceptability limits, 70% are within 90% acceptability limits and 5% coincide with the comfort temperature. In Model Type 2 (Figure 8b), 5% of the days in the summer period are outside the comfort range, 30% are

within 80% acceptability limits, 60% are within 90% acceptability limits and 5% of the days coincide with the comfort temperature.

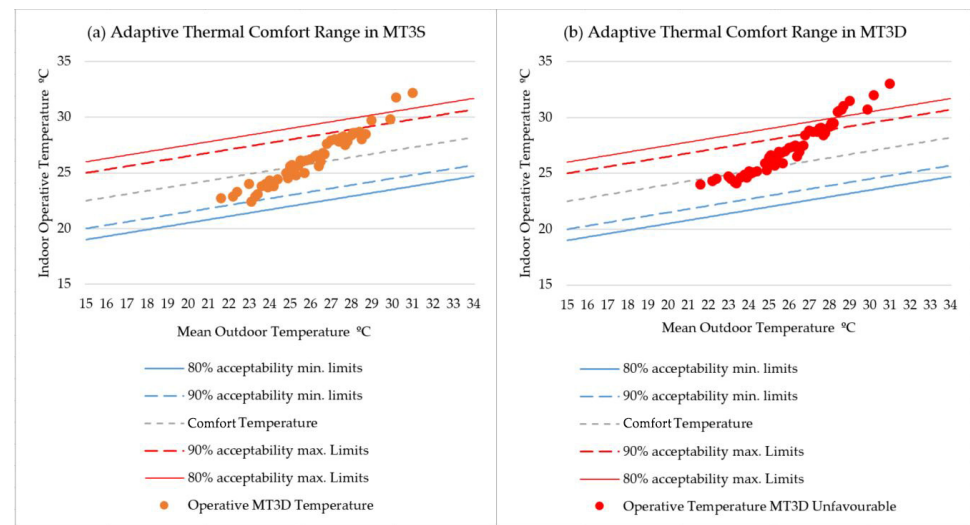


Figure 9. Adaptive thermal comfort in Simplified and Detailed Models Type 3 according to [22] ASHRAE 55. (a) Simplified Model Type 3. (b) Most unfavorable situation in Detailed Model Type 3.

The next stage was to look at the adaptive thermal comfort ranges for Simplified Model Type 3 and for the most unfavorable situation in Detailed Model Type 3, as established from the average outdoor temperature and the indoor operating temperature during the summer period. Figure 9a shows that, in Simplified Model Type 3, 5% of the days in the summer period are outside the comfort range, 5% are within the 80% acceptability limits, 80% are within 90% acceptability limits and 10% of the days coincide with the comfort temperature. Figure 9b shows the results for the unfavorable situation in Detailed Model Type 3. In this case, 20% of the days are outside the comfort range, 20% are within 80% acceptability limits, 39% are within 90% acceptability limits and 10% of the days coincide with the comfort temperature. It should be noted that, in both cases, the acceptability percentages only refer to the maximum limits because there are no values less than the ideal comfort temperature.

6. Discussion

6.1. Characterization of Models, Simulation Setup, and Study Limitations

The decisions made during the simulation ensure the obtainment of reliable results. One of these decisions involves verifying the temperature difference between the climatic data file and the data collected during the monitoring campaign, ensuring it does not exceed 3 °C. Regarding the interior temperatures of the models, they undergo a thorough and detailed calibration and validation process following ASHRAE 14 (2014) [105] for greater precision in the results. Additionally, the models include the thermal bridges existing at the junctions between different construction elements and are simulated using the most commonly used calculation engine in simulation literature, EnergyPlus, through the OpenStudio application for SketchUp, incorporating ASHRAE 55 (2020) [22] criteria. As for the study's limitations, the models do not account for ambient humidity or its transfer through construction elements due to a lack of means for measurement.

6.2. Influence of U-Factor and Orientation in the Models

The results confirm that smaller façades are associated with a low WWR, as is the case in Model Type 1 and in the west façade of Model Type 2. For the same WWR range, higher U-factor values are detected on the west façade and lower ones on the south façade of Model Type 1, which implies that the south façade of Model Type 1 has the best thermal behavior. U-factor values increase in line with increases in WWR, which is why, in Models

Type 2 and 3, the north and east façades, which have the highest WWR, also have a slightly higher U-factor. The west façade, however, which has a lower WWR, has a correspondingly lower U-factor, thus worsening its thermal behavior. The eastern façade of Model Type 2, which is in the highest WWR range, has the highest U-factor.

Regarding compliance with the U factor limits established by CTE DB HE (2022) [31], we found that the values for the exterior walls of the three models do not comply with the limits established by the CTE and that the thermal response improves in line with the thickness of the walls. The roofs do not meet the limits required by the CTE either, although the flat roof in Models Type 1 and 3 behaves better than the sloped roof in Model Type 2. The floors in all three types of farmhouses have the same characteristics and good thermal behavior, unlike the walls and roofs. Table 4 shows that, in general terms, the U factor values are between 30 and 40% of the limit value, with the exception of the east and north façades in Model Type 2, the façades with the highest WWR values in the study, which reach 75 and 93% of the limit values, respectively.

These results show that the south- and east-facing façades perform best, so confirming the findings of [106,107], for whom the south-facing façades achieved the best results, unlike [108]. In addition, north-facing façades with a low WWR obtained similar results to the south- and east-facing façades, so confirming the findings of [23].

6.3. Behavior of Models in the Face of Extreme Temperatures

The results of our research highlight that the traditional farmhouses in the study area behave well in the face of the extreme temperatures to which they are exposed during the summer months. The three models demonstrate their ability to mitigate a certain amount of heat when maximum temperatures are reached outside. Model Type 2 shows the best performance in this situation, reducing the maximum outside temperature by up to 10.1 °C, which makes it the most favorable case when the outside temperature increases. For its part, Model Type 1 shows the lowest mitigation capacity, reducing this temperature by 9.2 °C. Simplified Model Type 3 achieved similar results to Model Type 1, with a maximum temperature reduction of 8.3 °C compared with the maximum outside temperature.

However, to obtain a complete vision of Model Type 3, the results for the simplified version must be compared with those for the detailed version. The results show that the space that behaves worst in the face of extreme outdoor temperatures is located on the upper floor, which is incapable of mitigating the heat. By contrast, on the ground floor, the space with the best thermal behavior manages to reduce the highest temperatures by up to 9.6 °C. In short, Detailed Model Type 3 has worse results because its top floor has a larger area exposed to the elements. By contrast, the ground floor is quite well protected from them by the upper floor. This is because the upper floor acts as an air chamber between the outside and the ground floor, providing thermal insulation.

6.4. Adaptive Thermal Comfort in Standard Models According to ASHRAE 55

In general, the operation of the models is highly satisfactory during the summer period according to the ASHRAE 55 (2020) [22] guidelines; the results clearly demonstrate the thermal capacity of the architectural typology. In the adaptive thermal comfort study, Models Type 1 and Type 2 had a high percentage of operating temperatures within the acceptability limit of 90%, in line with [109]. However, unlike [110], there are some days within the summer period in which the operating temperature does not meet the acceptability limit of 80%. With respect to the Model 3, it is proven that the Simplified Model has 30% more days with operating temperatures within comfort limits compared with the Detailed Model. In line with [111], the average operating temperature for the Simplified Model falls within the 80% acceptability limit, a situation that does not apply to the Detailed Model, where, in line with [101], the average operating temperature exceeds this limit. On the other hand, the Simplified Model is more compliant with the limits of ASHRAE 55 (2020) [22] compared with the Detailed Type. In line with [111], the Simplified Model meets the limits for an

additional 15% of days more than the Detailed Model. Instead, this Detailed Model Model agrees with [108] in exceeding these limits frequently.

7. Conclusions

Within the current context of climate change, the decision-making process must be guided towards bioclimatic design and existing built heritage must be adapted to help mitigate the effects of global warming. With this in mind, energy simulations can be carried out on existing buildings so as to assess their thermal conditions and energy efficiency and decide what measures must be taken within the guidelines established by the regulatory framework. To this end, in this research, we evaluated the impact of the Mediterranean climate on representative models of traditional Mediterranean architecture in general and of the Eastern Almería farmhouse in particular. The results highlight the benefits of buildings of this kind which apply passive strategies to mitigate the extreme temperatures being produced by climate change.

The main conclusions obtained are as follows:

- Regarding orientation, WWR and U-factor values, it can be deduced that the smaller the surface area of the façade, the lower its WWR tends to be, which results in a lower U-factor and better thermal capacity.
- It should be noted that in façades with similar WWR values, the most favorable orientation is south and the most unfavorable is west. Despite this, all the façades met the limits established by CTE DB HE (2022) [31].
- The modeling phase is a crucial factor in the simulation to obtain reliable indoor temperatures, a necessary condition for the preservation of the built heritage [112]. This includes the process of calibrating and validating the models, as well as characterizing thermal bridges.
- The indoor temperature values of the models were obtained by simulation. The results show that farmhouses with compact floor plans and sloping roofs (Model Type 2) have the greatest thermal capacity to mitigate the extremely high outdoor temperatures in the summer in the study area. By contrast, the worst response to extreme temperatures was obtained in farmhouses composed by addition disaggregated rooms on the top floor (Detailed Model Type 3).
- In the two-story farmhouses (Model Type 3), the thermal capacity of the walls, roofs and ceilings of the upper floor creates an air chamber that increases the difference between the extreme exterior temperature and the interior temperature of the ground floor. However, the difference between the exterior temperature and the interior temperature of the upper floor is not as noticeable.
- The thermal comfort assessed according to the ASHRAE 55 (2020) [22] guidelines confirms that in farmhouses with compact floor plans and sloping roofs (Model Type 2), the temperature is maintained within the established acceptability limits for a longer period. According to these same guidelines, the compact farmhouses (Model Type 1) are the ones with the worst response. The compact farmhouse and most of the rooms of the disagggregated farmhouses (Models Type 1, Type 2 and Simplified Model Type 3) meet the requirements of ASHRAE 55 (2020) [22] for more than half the summer period, a situation that does not occur in the most unfavorable room of the disaggregated farmhouse (Detailed Model Type 3).

This study confirms that the different types of farmhouses studied have sufficient thermal capacities to respond to the climatic conditions of Eastern Almería, which gives them added value in addition to their importance as heritage buildings. Thus, vernacular architecture and historic buildings demonstrate great thermal capacity facing extreme temperatures, thanks to the materials of their construction elements, the thickness of their envelopes and the orientation of their façades. Therefore, the results obtained can be used as a guide for designers and construction industry investors, in order to pursue projectual solutions that appropriately reflect the current market needs of high energy performance of the built environment. The research carried out shows that traditional

Mediterranean architecture has the necessary thermal properties for the climate in this region, demonstrating that the particular characteristics of these buildings enhance thermal comfort inside them. This research could be expanded by analyzing a longer period of time and extending it to different typologies, climates and locations. Future insights could provide for the implementation of sensitivity analysis and/or threshold analysis for different values of the considered energetic parameters, in order to verify the robustness of the developed models. This would enable us to validate this method for evaluating the bioclimatic design of traditional buildings, so that they can be taken into account in future regulations and guidelines for mitigating the impact of climate change in existing buildings.

Author Contributions: Conceptualization, M.P.S.-P., L.M.G.R. and F.T.; methodology, M.P.S.-P. and L.M.G.R.; validation, M.P.S.-P. and L.M.G.R.; formal analysis, M.P.S.-P. and L.M.G.R.; investigation, M.P.S.-P., L.M.G.R. and F.T.; resources, M.P.S.-P. and L.M.G.R.; data curation M.P.S.-P. and L.M.G.R.; writing—original draft preparation, M.P.S.-P., L.M.G.R. and F.T.; writing—review and editing, M.P.S.-P., L.M.G.R. and F.T.; visualization, M.P.S.-P., L.M.G.R. and F.T.; supervision, M.P.S.-P. and L.M.G.R.; project administration, M.P.S.-P. and L.M.G.R. All authors have read and agreed to the published version of the manuscript.

Funding: This research was funded by the University of Granada and the Vicerrectorado de Investigación y Transferencia, with the project PP2022.PP.27 belonging to the Research and Transfer Plan.

Institutional Review Board Statement: Not applicable.

Informed Consent Statement: Not applicable.

Data Availability Statement: No new data were created or analyzed in this study. Data sharing is not applicable to this article.

Acknowledgments: The authors would like to thank the reviewers for their thoughtful comments and efforts towards improving our manuscript. This work was supported by the collaboration of the projects REMINE Programme for Research and Innovation Horizon 2020 Marie Skłodowska-Curie Actions, WARMEST Research and Innovation Staff Exchange (RISE) H2020-MSCA-RISE-2017, RRRMAKER H2020- MSCA-RISE-2020 Marie Skłodowska-Curie Research and Innovation Staff Exchange and Scientific Unit of excellence “Ciencia en la Alhambra”, ref. UCE-PP2018-01, University of Granada. The research was carried out under the auspices of Research Groups RNM 0179 and HUM 629 of the Junta de Andalucía.

Conflicts of Interest: The authors declare no conflicts of interest.

Abbreviations

e	Thickness (m)
h	Width (m)
HVAC	Heating, Ventilation and Air Conditioning
R _{se}	Outdoor Air Superficial Thermal Resistance (m ² K/W)
R _{si}	Indoor Air Superficial Thermal Resistance (m ² K/W)
R _t	Superficial Thermal Resistance (m ² K/W)
SDG	Sustainable Development Goal
S _f	Façade area (m ²)
S _w	Window area (m ²)
T ₀	Operative temperature (°C)
T _{MT}	Indoor temperature of the Model Type (°C)
T _{med}	Average indoor temperature
U-factor	Superficial Thermal Transmittance (W/m ² K)
U _{HI}	Urban Heat Island
U _P	Equivalent superficial Thermal Transmittance of the thermal bridge (W/m ² K)
WWR	Window-to-Wall Ratio
λ	Thermal conductivity (W/mK)
Ψ	Linear thermal transmittance (W/mK)

References

1. Ciancio, V.; Salata, F.; Falasca, S.; Curci, G.; Golasi, I.; de Wilde, P. Energy demands of buildings in the framework of climate change: An investigation across Europe. *Sustain. Cities Soc.* **2020**, *60*, 102213. [CrossRef]
2. D'Agostino, D.; Parker, D.; Epifani, I.; Crawley, D.; Lawrie, L. How will future climate impact the design and performance of nearly Zero Energy Buildings (nZEBs)? *Energy* **2022**, *240*, 122479. [CrossRef]
3. Qian, W.; Li, X. A cold island connectivity and network perspective to mitigate the urban heat island effect. *Sustain. Cities Soc.* **2023**, *94*, 104525. [CrossRef]
4. Salata, F.; Falasca, S.; Ciancio, V.; Curci, G.; de Wilde, P. Climate-change related evolution of future building cooling energy demand in a Mediterranean Country. *Energy Build.* **2023**, *290*, 113112. [CrossRef]
5. Xiong, J.; Guo, S.; Wu, Y.; Yan, D.; Xiao, C.; Lu, X. Predicting the response of heating and cooling demands of residential buildings with various thermal performances in China to climate change. *Energy* **2023**, *269*, 126789. [CrossRef]
6. Sustainable Development Goals. Available online: <https://www.un.org/sustainabledevelopment/> (accessed on 9 July 2023).
7. Bardhan, R.; Debnath, R.; Gama, J.; Vijay, U. REST framework: A modelling approach towards cooling energy stress mitigation plans for future cities in warming Global South. *Sustain. Cities Soc.* **2020**, *61*, 102315. [CrossRef]
8. Cholewa, T.; Siuta-Olcha, A.; Smolarz, A.; Muryjas, P.; Wolszczak, P.; Guz, Ł.; Bocian, M.; Sadowska, G.; Łokczewska, W.; Balaras, C.A. On the forecast control of heating system as an easily applicable measure to increase energy efficiency in existing buildings: Long term field evaluation. *Energy Build.* **2023**, *292*, 113174. [CrossRef]
9. Adly, B.; El-Khouly, T. Combining retrofitting techniques, renewable energy resources and regulations for residential buildings to achieve energy efficiency in gated communities. *Ain Shams Eng. J.* **2022**, *13*, 101772. [CrossRef]
10. Bui, D.K.; Nguyen, T.N.; Ghazlan, A.; Ngo, T.D. Biomimetic adaptive electrochromic windows for enhancing building energy efficiency. *Appl. Energy* **2021**, *300*, 117341. [CrossRef]
11. Song, K.; Jang, Y.; Park, M.; Lee, H.S.; Ahn, J. Energy efficiency of end-user groups for personalized HVAC control in multi-zone buildings. *Energy* **2020**, *206*, 118116. [CrossRef]
12. Vieites, E.; Vassileva, I.; Ariasa, J.E. European initiatives towards improving the energy efficiency in existing and historic buildings. *Energy Procedia* **2015**, *75*, 1679–1685. [CrossRef]
13. Wani, M.; Hafiz, F.; Swain, A.; Ukil, A. Estimating thermal parameters of a commercial building: A meta-heuristic approach. *Energy Build.* **2021**, *231*, 110537. [CrossRef]
14. Rabl, A. Parameter estimation in buildings: Methods for dynamic analysis of measured energy use. *J. Sol. Energy Soc.* **1988**, *110*, 52–66. [CrossRef]
15. Dewson, T.; Day, B.; Irving, A. Least squares parameter estimation of a reduced order thermal model of an experimental building. *Build. Environ.* **1993**, *28*, 127–137. [CrossRef]
16. Chen, T.; Athienitis, A. Investigation of practical issues in building thermal parameter estimation. *Build. Environ.* **2003**, *38*, 1027–1038. [CrossRef]
17. Wang, S.; Xu, X. Parameter estimation of internal thermal mass of building dynamic models using genetic algorithm. *Energy Convers.* **2006**, *47*, 1927–1941. [CrossRef]
18. Castillo, L.; Enríquez, R.; Jiménez, M.; Heras, M. Dynamic integrated method based on regression and averages, applied to estimate the thermal parameters of a room in an occupied office building in Madrid. *Energy Build.* **2014**, *81*, 337–362. [CrossRef]
19. Yang, Z.; Li, X.; Lu, Y.; Bowers, C.; Schnier, T.; Tang, K.; Yao, X. An efficient evolutionary approach to parameter identification in a building thermal model. *IEEE Trans. Syst. Man Cybern. Syst.* **2011**, *42*, 957–969. [CrossRef]
20. Bouache, T.; Limam, K.; Bosschaerts, W. New thermal parameters identification approach applied to the thermal renovation of buildings. *Energy Build.* **2015**, *104*, 156–164. [CrossRef]
21. Yang, X.; Peng, L.L.H.; Jiang, Z.; Chen, Y.; Yao, L.; He, Y.; Xu, T. Impact of urban heat island on energy demand in buildings: Local climate zones in Nanjing. *Appl. Energy* **2020**, *260*, 114279. [CrossRef]
22. ANSI; ASHRAE. *Standard 55: Thermal Environmental Conditions for Human Occupancy*; ASHRAE: Peachtree Corners, Georgia, 2020.
23. Chi, F.; Wang, Y.; Wang, R.; Li, G.; Peng, C. An investigation of optimal window-to-wall ratio based on changes in building orientations for traditional dwellings. *Sol. Energy* **2020**, *195*, 64–81. [CrossRef]
24. Ma, R.; Ma, R.; Long, E. Analysis of the rule of window-to-wall ratio on energy demand of residential buildings in different locations in China. *Heliyon* **2023**, *9*, e12803. [CrossRef] [PubMed]
25. Xie, X.; Chen, X.; Xu, B.; Pei, G. Investigation of occupied/unoccupied period on thermal comfort in Guangzhou: Challenges and opportunities of public buildings with high window-wall ratio. *Energy* **2022**, *244*, 123186. [CrossRef]
26. Szcześniak, J.T.; Ang, Y.Q.; Letellier-Duchesne, S.; Reinhart, C.F. A method for using street view imagery to auto-extract window-to-wall ratios and its relevance for urban-level daylighting and energy simulations. *Build. Environ.* **2022**, *207*, 108108. [CrossRef]
27. Liang, Y.; Pan, Y.; Yuan, X.; Yang, Y.; Fu, L.; Li, J.; Sun, T.; Huang, Z.; Kosonen, R. Assessment of operational carbon emission reduction of energy conservation measures for commercial buildings: Model development. *Energy Build.* **2022**, *268*, 112189. [CrossRef]

28. Peng, J.; Curcija, D.C.; Thanachareonkit, A.; Lee, E.S.; Goudey, H.; Jonsson, J.; Selkowitz, S.E. Comparative study on the overall energy performance between photovoltaic and Low-E insulated glass units. *Sol. Energy* **2021**, *214*, 443–456. [[CrossRef](#)]
29. Maučec, D.; Premrov, M.; Leskovar, V.Ž. Use of sensitivity analysis for a determination of dominant design parameters affecting energy efficiency of timber buildings in different climates. *Energy Sustain. Dev.* **2021**, *63*, 86–102. [[CrossRef](#)]
30. Rajput, M.; Augenbroe, G.; Stone, B.; Georgescu, M.; Broadbent, A.; Krayenhoff, S.; Mallen, E. Heat exposure during a power outage: A simulation study of residences across the metro Phoenix area. *Energy Build.* **2022**, *259*, 111605. [[CrossRef](#)]
31. Código Técnico de la Edificación. *Documento Básico de Ahorro de Energía*; Ministerio de Transportes, Movilidad y Agenda Urbana: Madrid, Spain, 2022.
32. Lassandro, S.; Turi, D. Multi-criteria and multiscale assessment of building envelope response-ability to rising heat waves. *Sustain. Cities Soc.* **2019**, *51*, 101755. [[CrossRef](#)]
33. Wang, V.R.; Lu, S.; Feng, W.; Xu, B. Tradeoff between heating energy demand in winter and indoor overheating risk in summer constrained by building standards. *Build. Simul.* **2021**, *14*, 987–1003. [[CrossRef](#)]
34. Tol, H.I.; Madessa, H.B. Development of a white-box dynamic building thermal model integrated with a heating system. *J. Build. Eng.* **2023**, *68*, 106038. [[CrossRef](#)]
35. François, A.; Ibos, L.; Feuillet, V.; Meulemans, J. Estimation of the thermal resistance of a building wall with inverse techniques based on rapid active in situ measurements and white-box or ARX black-box models. *Energy Build.* **2020**, *226*, 110346. [[CrossRef](#)]
36. Kefer, K.; Hanghofer, R.; Kefer, P.; Stöger, M.; Hofer, B.; Affenzeller, M.; Winkler, S. Simulation-Based Optimization of Residential Energy Flows Using White Box Modeling by Genetic Programming. *Energy Build.* **2022**, *258*, 111829. [[CrossRef](#)]
37. Nie, V.Z.; Chen, S.; Zhang, S.; Wu, H.; Weiss, T.; Zhao, L. Adaptive Façades Strategy: An architect-friendly computational approach based on co-simulation and white-box models for the early design stage. *Energy Build.* **2023**, *296*, 113320. [[CrossRef](#)]
38. D’Agostino, D. Assessment of the progress towards the establishment of definitions of Nearly Zero Energy Buildings (nZEBs) in European Member States. *J. Build. Eng.* **2015**, *1*, 20–32. [[CrossRef](#)]
39. Ghoreishi, K.; Fernández-Gutiérrez, A.; Fernández-Hernández, F.; Parras, L. Retrofit planning and execution of a Mediterranean villa using on-site measurements and simulations. *J. Build. Eng.* **2021**, *35*, 102083. [[CrossRef](#)]
40. Amecke, H. The impact of energy performance certificates: A survey of German homeowners. *Energy Policy* **2012**, *46*, 4–14. [[CrossRef](#)]
41. Murphy, L. The Influence of the Energy Performance Certificate: The Dutch Case. *Energy Policy* **2014**, *67*, 664–672. [[CrossRef](#)]
42. Morano, P.; Tajani, F.; Di Liddo, F.; Guarnaccia, C. The value of the energy retrofit in the Italian housing market: Two case-studies compared. *WSEAS Trans. Bus. Econ.* **2018**, *15*, 249–258.
43. Manganelli, B.; Morano, P.; Tajani, F.; Salvo, F. Affordability assessment of energy-efficient building construction in Italy. *Sustainability* **2019**, *11*, 249. [[CrossRef](#)]
44. Annibaldi, V.; Cucchiella, F.; Rotilio, M. Economic and environmental assessment of thermal insulation. A case study in the Italian context. *Case Stud. Constr. Mater.* **2021**, *15*, e00682. [[CrossRef](#)]
45. Maaouane, M.; Chennaif, M.; Zouggar, S.; Krajačić, G.; Amrani, S.; Zahboune, S. Cost-effective design of energy efficiency measures in the building sector in North Africa using Building Information Modeling. *Energy Build.* **2023**, *294*, 113283. [[CrossRef](#)]
46. Mayer, K.; Haas, L.; Huang, T.; Bernabé-Moreno, J.; Rajagopal, R.; Fischer, M. Estimating building energy efficiency from street view imagery, aerial imagery, and land surface temperature data. *Appl. Energy* **2023**, *333*, 120542. [[CrossRef](#)]
47. D’Ambrosio Alfano, F.R.; Olesen, B.W.; Palella, B.I.; Riccio, G. Thermal comfort: Design and assessment for energy saving. *Energy Build.* **2014**, *81*, 326–336. [[CrossRef](#)]
48. Ascione, F.; De Masi, R.F.; De Rossi, F.; Ruggiero, S.; Vanoli, G.P. Optimization of building envelope design for nZEBs in Mediterranean climate: Performance analysis of residential case study. *Appl. Energy* **2016**, *183*, 938–957. [[CrossRef](#)]
49. Bakonyi, D.; Dobszay, G. Simulation aided optimization of a historic window’s refurbishment. *Energy Build.* **2016**, *126*, 51–69. [[CrossRef](#)]
50. Alongi, A.; Scoccia, R.; Motta, M.; Mazzarella, L. Numerical investigation of the Castle of Zena energy needs and a feasibility study for the implementation of electric and gas driven heat pump. *Energy Build.* **2015**, *95*, 32–38. [[CrossRef](#)]
51. Pisello, A.L.; Petrozzi, A.; Castaldo, V.L.; Cotana, F. Energy refurbishment of historical buildings with public function: Pilot case study. *Energy Procedia* **2014**, *61*, 660–663. [[CrossRef](#)]
52. Pisello, A.L.; Petrozzi, A.; Castaldo, V.L.; Cotana, F. On an innovative integrated technique for energy refurbishment of historical buildings: Thermal-energy, economic and environmental analysis of a case study. *Appl. Energy* **2016**, *162*, 1313–1322. [[CrossRef](#)]
53. Atmaca, A.B.; Gedik, G.Z. Determination of thermal comfort of religious buildings by measurement and survey methods: Examples of mosques in a temperate-humid climate. *J. Build. Eng.* **2020**, *30*, 101246. [[CrossRef](#)]
54. Mauri, L. Feasibility analysis of retrofit strategies for the achievement of NZEB target on a historic building for tertiary use. *Energy Procedia* **2016**, *101*, 1127–1134. [[CrossRef](#)]
55. Etxebarria Mallea, M.; Etxepare Igiñiz, L.; De Luxán De Diego, M. Passive hygrothermal behaviour and indoor comfort concerning the construction evolution of the traditional Basque architectural model. Lea valley case study. *Build. Environ.* **2018**, *143*, 496–512. [[CrossRef](#)]
56. Manzano-Agugliaro, F.; Montoya, F.G.; Sabio-Ortega, A.; García-Cruz, A. Review of bioclimatic architecture strategies for achieving thermal comfort. *Renew. Sustain. Energy Rev.* **2015**, *49*, 736–755. [[CrossRef](#)]

57. Bodach, S.; Lang, W.; Hamhaber, J. Climate responsive building design strategies of vernacular architecture in Nepal. *Energy Build.* **2014**, *81*, 227–242. [[CrossRef](#)]
58. Cano, M.; Garzón, E.; Sánchez-Soto, P.J. Historic preservation, GIS, & rural development: The case of Almería province, Spain. *Appl. Geogr.* **2013**, *42*, 34–47. [[CrossRef](#)]
59. García-Ruiz, L.M.; Sáez-Pérez, M.P.; Verdú-Vázquez, A. Viability in heritage vs necessity of intervention. Viable project in The Cortijo del Fraile in Níjar. *Anales de Edificación* **2019**, *5*, 66–75. [[CrossRef](#)]
60. Sáez-Pérez, M.P.; García-Ruiz, L.M. Structural characterisation and numerical assessment of seismic damage of the Cortijo del Fraile farmhouse in Níjar (Almería, Spain). *Tecnol. De La Construcción* **2020**, *95*, 252–256. [[CrossRef](#)]
61. Calama-González, C.M.; Escandón, R.; Alonso, A.; Suárez, R.; León-Rodríguez, A.L.; Gutiérrez, A.S.; Arriazu-Ramos, A.; Monge-Barrio, A. Thermal insulation impact on overheating vulnerability reduction in Mediterranean dwellings. *Heliyon* **2023**, *9*, e16102. [[CrossRef](#)] [[PubMed](#)]
62. Timur, B.A.; Başaran, T.; İpekoğlu, B. Thermal retrofitting for sustainable use of traditional dwellings in Mediterranean climate of southwestern Anatolia. *Energy Build.* **2022**, *256*, 111712. [[CrossRef](#)]
63. Philokyprou, M.; Michael, A.; Malaktou, E.; Savvides, A. Environmentally responsive design in Eastern Mediterranean. The case of vernacular architecture in the coastal, lowland and mountainous regions of Cyprus. *Build. Environ.* **2017**, *111*, 91–109. [[CrossRef](#)]
64. Caro, R.; Sendra, J.J. Are the dwellings of historic Mediterranean cities cold in winter? A field assessment on their indoor environment and energy performance. *Energy Build.* **2021**, *230*, 110567. [[CrossRef](#)]
65. Abela, A.; Hoxley, M.; McGrath, P.; Goodhew, S. An investigation of the appropriateness of current methodologies for energy certification of Mediterranean housing. *Energy Build.* **2016**, *130*, 210–218. [[CrossRef](#)]
66. Guillén-Lambea, S.; Rodríguez-Soria, B.; Marín, J.M. Evaluation of the potential energy recovery for ventilation air in dwellings in the South of Europe. *Energy Build.* **2016**, *128*, 384–393. [[CrossRef](#)]
67. Posani, M.; Veiga, R.; Freitas, V. Post-Insulating traditional massive walls in Southern Europe: A moderate thermal resistance can be more effective than you think. *Energy Build.* **2023**, *295*, 113299. [[CrossRef](#)]
68. Zhao, M.; Mehra, S.R.; Künzle, H.M. Energy-saving potential of deeply retrofitting building enclosures of traditional courtyard houses—A case study in the Chinese Hot-Summer-Cold-Winter zone. *Build. Environ.* **2022**, *217*, 109106. [[CrossRef](#)]
69. Jiang, W.; Ju, Z.; Tian, H.; Liu, Y.; Arıcı, M.; Tang, X.; Li, Q.; Li, D.; Qi, H. Net-zero energy retrofit of rural house in severe cold region based on passive insulation and BAPV technology. *J. Clean. Prod.* **2022**, *360*, 132198. [[CrossRef](#)]
70. Laib, I.; Hamidat, A.; Haddadi, M.; Ramzan, N.; Olabi, A.G. Study and simulation of the energy performances of a grid-connected PV system supplying a residential house in north of Algeria. *Energy* **2018**, *152*, 445–454. [[CrossRef](#)]
71. Jasha, T.A.; Iqbal, M.T. Thermal Simulation and Energy Consumption Analysis of Two Houses in St. John’s, Newfoundland. *Procedia Eng.* **2015**, *105*, 607–612. [[CrossRef](#)]
72. Porsani, G.B.; Casquero-Modrego, N.; Trueba, J.B.E.; Bandera, C.F. Empirical evaluation of EnergyPlus infiltration model for a case study in a high-rise residential building. *Energy Build.* **2023**, *296*, 113322. [[CrossRef](#)]
73. Ciardiello, A.; Rosso, F.; Dell’Olmio, J.; Ciancio, V.; Ferrero, M.; Salata, F. Multi-objective approach to the optimization of shape and envelope in building energy design. *Appl. Energy* **2020**, *280*, 115984. [[CrossRef](#)]
74. Ng, L.C.; Dols, W.S.; Emmerich, S.J. Evaluating potential benefits of air barriers in commercial buildings using NIST infiltration correlations in EnergyPlus. *Build. Environ.* **2021**, *196*, 107783. [[CrossRef](#)]
75. Liu, Z.; Hou, J.; Zhang, L.; Dewancker, B.J.; Meng, X.; Hou, C. Research on energy-saving factors adaptability of exterior envelopes of university teaching-office buildings under different climates (China) based on orthogonal design and EnergyPlus. *Heliyon* **2022**, *8*, e10056. [[CrossRef](#)]
76. Feng, F.; Fu, Y.; Yang, Z.; O’Neill, Z. Enhancement of phase change material hysteresis model: A case study of modeling building envelope in EnergyPlus. *Energy Build.* **2022**, *276*, 112511. [[CrossRef](#)]
77. Park, M.; Wang, Z.; Li, L.; Wang, X. Multi-objective building energy system optimization considering EV infrastructure. *Appl. Energy* **2023**, *332*, 120504. [[CrossRef](#)]
78. Elsharkawy, H.; Zahiri, S. The significance of occupancy profiles in determining post retrofit indoor thermal comfort, overheating risk and building energy performance. *Build. Environ.* **2020**, *172*, 106676. [[CrossRef](#)]
79. Leccese, F.; Salvadori, G.; Asdrubali, F.; Gori, P. Passive thermal behaviour of buildings: Performance of external multilayered walls and influence of internal walls. *Appl. Energy* **2018**, *225*, 1078–1089. [[CrossRef](#)]
80. Sakiyama, N.R.M.; Mazzaferro, L.; Carlo, J.C.; Bejat, T.; Garrecht, H. Natural ventilation potential from weather analyses and building Simulation. *Energy Build.* **2021**, *231*, 110596. [[CrossRef](#)]
81. Guo, W.; Liang, S.; He, Y.; Li, W.; Xiong, B.; Wen, H. Combining EnergyPlus and CFD to predict and optimize the passive ventilation mode of medium-sized gymnasium in subtropical regions. *Build. Environ.* **2022**, *207*, 108420. [[CrossRef](#)]
82. Alonso, M.J.; Dols, W.S.; Mathisen, H.M. Using Co-simulation between EnergyPlus and CONTAM to evaluate recirculation-based, demand-controlled ventilation strategies in an office building. *Build. Environ.* **2022**, *211*, 108737. [[CrossRef](#)]
83. Pandey, B.; Banerjee, B.; Sharma, A. Coupled EnergyPlus and CFD analysis of PCM for thermal management of buildings. *Energy Build.* **2021**, *231*, 110598. [[CrossRef](#)]

84. Strand, R.K. Incorporating two-dimensional conduction modeling techniques into an energy simulation program: The EnergyPlus radiant system example. *Energy Build.* **2022**, *274*, 112405. [[CrossRef](#)]
85. Wang, W.; Li, S.; Guo, S.; Ma, M.; Feng, S.; Bao, L. Benchmarking urban local weather with long-term monitoring compared with weather datasets from climate station and EnergyPlus weather (EPW) data. *Energy Rep.* **2021**, *7*, 6501–6514. [[CrossRef](#)]
86. Balaji, N.C.; Mani, M.; Reddy, B.V.V. Dynamic thermal performance of conventional and alternative building wall Envelopes. *J. Build. Eng.* **2019**, *21*, 373–395. [[CrossRef](#)]
87. Coelho, G.B.A.; Silva, H.E.; Henriques, F.M.A. Calibrated hygrothermal simulation models for historical buildings. *Build. Environ.* **2018**, *142*, 439–450. [[CrossRef](#)]
88. Tarek, D.; Ahmed, M.M.; Hussein, H.S.; Zeyad, A.M.; Al-Enizi, A.M.; Yousef, A.; Ragab, A. Building envelope optimization using geopolymer bricks to improve the energy efficiency of residential buildings in hot arid regions. *Case Stud. Constr. Mater.* **2022**, *17*, e01657. [[CrossRef](#)]
89. Vox, G.; Blanco, I.; Convertino, F.; Schettini, E. Heat transfer reduction in building envelope with green façade system: A year-round balance in Mediterranean climate conditions. *Energy Build.* **2022**, *174*, 112439. [[CrossRef](#)]
90. Martínez, R.; Arregi, B.; Lumbreras, M. Surface heat transfer coefficients in building envelopes: Uncertainty levels in experimental methods. *J. Build. Phys.* **2022**, *47*, 62–91. [[CrossRef](#)]
91. Agyekum, K.; Kissi, E.; Danku, J.C. Professionals' views of vernacular building materials and techniques for green building delivery in Ghana. *Sci. Afr. J. Sci.* **2020**, *8*, e00424. [[CrossRef](#)]
92. Ortega, J.; Vasconcelos, G.; Rodrigues, H.; Correia, M. A vulnerability index formulation for the seismic vulnerability assessment of vernacular architecture. *Eng. Struct.* **2019**, *197*, 109381. [[CrossRef](#)]
93. Philokyprou, M.; Michael, A.; Malaktou, E. A typological, environmental and socio-cultural study of semi-open spaces in the Eastern Mediterranean vernacular architecture: The case of Cyprus. *Front. Archit. Res.* **2021**, *10*, 483–501. [[CrossRef](#)]
94. Ozariso, B.; Altan, H. Systematic literature review of bioclimatic design elements: Theories, methodologies and cases in the South-eastern Mediterranean climate. *Energy Build.* **2021**, *250*, 111281. [[CrossRef](#)]
95. Bougiatioti, F.; Oikonomou, A. Architectural characteristics and environmental performance of byzantine houses and streets. *Build. Environ.* **2020**, *170*, 106605. [[CrossRef](#)]
96. Convertino, F.; Di Turi, S.; Stefanizzi, P. The color in the vernacular bioclimatic architecture in Mediterranean region. *Energy Procedia* **2017**, *126*, 211–218. [[CrossRef](#)]
97. Desogus, G.; Cannas, L.G.F.; Sanna, A. Bioclimatic lessons from Mediterranean vernacular architecture: The Sardinian case study. *Energy Build.* **2016**, *129*, 574–588. [[CrossRef](#)]
98. Lizana, J.; López-Cabeza, V.P.; Renaldi, R.; Diz-Mellado, E.; Rivera-Gómez, C.; Galán-Marín, C. Integrating courtyard microclimate in building performance to mitigate extreme urban heat impacts. *Sustain. Cities Soc.* **2022**, *78*, 103590. [[CrossRef](#)]
99. Diz-Mellado, E.; López-Cabeza, V.P.; Rivera-Gómez, C.; Galán-Marín, C.; Rojas-Fernández, J.; Nikolopoulou, M. Extending the adaptive thermal comfort models for courtyards. *Build. Environ.* **2021**, *203*, 108094. [[CrossRef](#)]
100. Salameh, M.M.; Touqan, B.A.; Awad, J.; Salameh, M.M. Heritage conservation as a bridge to sustainability assessing thermal performance and the preservation of identity through heritage conservation in the Mediterranean city of Nablus. *Ain Shams Eng. J.* **2022**, *13*, 101553. [[CrossRef](#)]
101. Thravalou, S.; Philokyprou, M. Urban design considerations in the environmental assessment of vernacular buildings with timber projections (sachnisi): The case of Nicosia's historic center. *Front. Archit. Res.* **2021**, *10*, 176–189. [[CrossRef](#)]
102. Pietrapertosa, F.; Olazabal, M.; Simoes, S.G.; Salvia, M.; Fokaides, P.A.; Ioannou, B.I.; Vigiú, V.; Spyridaki, N.A.; Hurtado, S.G.; Geneletti, D.; et al. Adaptation to climate change in cities of Mediterranean Europe. *Cities* **2023**, *140*, 104452. [[CrossRef](#)]
103. CTE WEB Prontuario de Soluciones Constructivas/Materiales. Available online: <http://cte-web.iccl.es/materiales.php?a=4> (accessed on 1 December 2021).
104. AEMET. Vicepresidencia Tercera del Gobierno de España. Ministerio para la Transición Ecológica y el Reto Demográfico. Agencia Estatal de Meteorología. Available online: <http://www.aemet.es> (accessed on 2 April 2023).
105. ANSI/ASHRAE Guideline 14-2014. Measurement of Energy, Demand and Water Savings. American Society of Heating, Ventilating and Air Conditioning Engineers (ASHRAE). Available online: www.ashrae.org/technology (accessed on 5 April 2022).
106. Mangkuto, R.A.; Tresna, D.N.A.T.; Hermawan, I.M.; Pradipta, J.; Jamala, N.; Paramita, B.; Atthailah. Experiment and simulation to determine the optimum orientation of building-integrated photovoltaic on tropical building façades considering annual daylight performance and energy yield. *Energy Built Environ.* **2024**, *5*, 414–425. [[CrossRef](#)]
107. Alumar, M.M.S. Understanding the environmental performance of the Iraqi traditional courtyard house, Is there an order of façades orientation in randomly oriented land plots? *J. Build. Eng.* **2019**, *22*, 140–146. [[CrossRef](#)]
108. Taleghani, M.; Swan, W.; Johansson, E.; Ji, Y. Urban cooling: Which façade orientation has the most impact on a microclimate? *Sustain. Cities Soc.* **2021**, *64*, 102547. [[CrossRef](#)]
109. Kajjoba, D.; Kasedde, H.; Olupot, P.W.; Lwanyaga, J.D. Evaluation of thermal comfort and air quality of low-income housing in Kampala City, Uganda. *Energy Built Environ.* **2022**, *3*, 508–524. [[CrossRef](#)]
110. Forcada, N.; Gangolells, M.; Casals, M.; Tejedor, B.; Macarulla, M.; Gaspar, K. Field study on adaptive thermal comfort models for nursing homes in the Mediterranean climate. *Energy Build.* **2021**, *252*, 111475. [[CrossRef](#)]

111. Wang, C.; Li, C.; Xie, L.; Wang, X.; Chang, L.; Wang, X.; Li, H.X.; Liu, Y. Thermal environment and thermal comfort in metro systems: A case study in severe cold region of China. *Build. Environ.* **2023**, *227*, 109758. [[CrossRef](#)]
112. Huerto-Cardenas, H.E.; Leonforte, F.; Aste, N.; Del Pero, C.; Evola, G.; Costanzo, V.; Lucci, E. Validation of dynamic hygrothermal simulation models for historical. *Build. Environ.* **2020**, *180*, 107081. [[CrossRef](#)]

Disclaimer/Publisher's Note: The statements, opinions and data contained in all publications are solely those of the individual author(s) and contributor(s) and not of MDPI and/or the editor(s). MDPI and/or the editor(s) disclaim responsibility for any injury to people or property resulting from any ideas, methods, instructions or products referred to in the content.